

Nanocavity strengthening: Impact of the broken bonds at the negatively curved surfaces

Yu Ding,¹ Chang Q. Sun,^{1,a)} and Y. C. Zhou²

¹*School of Electronic and Electrical Engineering, Nanyang Technological University of Singapore, Singapore 639798, Singapore*

²*Key Laboratory of Low-Dimensional Materials and Application Technologies, Xiangtan University, Ministry of Education, Hunan 411105, People's Republic of China*

(Received 26 September 2007; accepted 18 February 2008; published online 29 April 2008)

The atomistic origin of the atomic vacancy or nanocavity induced hardening in hollow nanotubes and nanoporous structures has long been a puzzle. An analysis from the perspective of bond-order-length-strength correlation mechanism [C. Q. Sun, *Prog. Solid State Chem.* **35**, 1 (2007)] has led to solutions that show that the shortened and strengthened bonds between the undercoordinated atoms in the negatively curved surface skins dominate the observed nanocavity strengthening and thermal instability of the porous structures. It is suggested that the broken bond derived local strain and quantum trapping and the associated energy densification provide pinning centers for inhibiting atomic dislocations and that the broken bond induced cohesive energy dropping dominate the thermal instability. On the other hand, nanocavities also provide sites that initiate the structure failure under plastic deformation. The agreement between predictions and the experimentally observed size dependence of mechanical strength of some nanoporous materials and the well-known phenomenon of hollow tube strengthening evidences for the proposed mechanism. © 2008 American Institute of Physics. [DOI: [10.1063/1.2907947](https://doi.org/10.1063/1.2907947)]

I. INTRODUCTION

It is expected that atomic vacancies or nanometric cavities reduce the number of chemical bonds of atoms nearby and, hence, the mechanical strength of the entire body of a hollow or a foamed structure. However, the hardness of a material with pores at the nanometer scale does not follow this picture of coordination counting unless an excessive amount of cavities¹ is involved or the pores are too large. The mechanical strength of metallic foams with micrometer-sized pores follows exceedingly well the well-known scaling laws of porosity induced strength weakening.²⁻⁶ It has long been realized^{7,8} that atomic vacancies or point defects could instead act as pinning centers that inhibit the motion of dislocations and, hence, enhance the mechanical strength of a material with a certain amount of defects with a physical origin that is yet unclear. Introduction of a limited amount of atomic vacancies or nanocavities could also enhance the mechanical strength of porous specimens. For instance, the hardness of FeAlN is proportional to the square root of the concentration of nitrogen vacancies⁹ and the hardness of WAIC monotonically increases up to a maximum at 35% carbon vacancies.¹ Fracture measurement and modeling analysis indicated that a small number of atomic defects could modulate the strength of WS₂ nanotubes.¹⁰ More recently, Wu and Dzenis¹¹ investigated the size effect on the elastic behavior of solid and hollow polymer nanofibers under uniaxial tension and they found that the fiber radius has an appreciable effect on the elastic response of polymer nanofibers. The smaller the fiber diameter is, the stronger the fibers will be.

Comparatively, a hollow nanofiber shows a greater stiffening effect with increasing axial stretch than the solid fiber of the same diameter, suggesting the significance of the negatively curved interior fiber skin. Carbon nanotubes with impurity-free atomic shells are ideal cases of cylindrical nanocavities that are much stronger than the bulk materials unless excessive defects are involved in the wall of the single-walled tubes.^{12,13} For instance, introduction of vacancies to unreconstructed single-walled nanotubes will decrease the tensile strength and critical strain of the nanotubes by nearly a factor of 2.¹⁴ The excessive defects on the wall act as centers that initiate mechanical failure. A theoretical calculation¹⁵ of the tensile strength of nanotube mats and fibers predicted that the stiffness and strength of the mats can be increased by at least an order in magnitude through small dose irradiation with energetic particles to break some bonds and generate some new interlayer bonds of the nanotubes.¹⁶ The internal stress of an amorphous carbon film can also be raised from 1 to 12 GPa by producing nanometric pores by using noble gas (Ar, Kr, and Xe) bombardment during film deposition.¹⁷⁻²⁰ One nanometer-sized gas bubble production by He implantation also enhances the hardness of Ni films from 1.1 to 8.3 GPa and the yield stress from 0.15 to 2.9 GPa.²¹

Nanofoamed materials that can be envisioned as a three-dimensional network of ultrahigh-strength nanowires or ligaments or spherical holes in the matrix are measured to be stiffer at low temperatures and tougher at raised temperatures compared to bulk crystals.²²⁻²⁶ Typically, the surface of an open-celled Au foam of an ~30% relative density is stronger than the foam interior and the foams made of smaller ligaments are even stiffer compared to the bulk.²⁷⁻³⁰ The hardness of an open-cell nanoporous Au has a value of some ten

^{a)}Electronic mail: ecqsun@ntu.edu.sg.

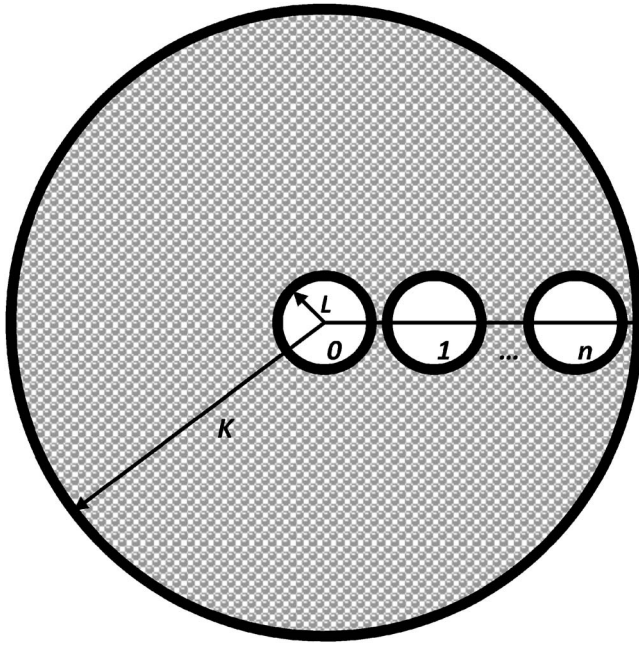


FIG. 1. Schematic illustration of the surface-to-volume ratio of a sphere with $4\pi(n+1/2)^2/3$ cavities and the three-phase structures, i.e., voids, skins, and the matrix. Only atoms in the dark skins contribute to the property change yet atoms in the core matrix remain as they are in the bulk.

times higher than the hardness³¹ predicted by the scaling laws²⁻⁶ for micrometer-sized porous structures. The compacted nanocrystalline Au ligaments exhibit an average grain size of <50 nm with hardness values ranging from 1.4 to 2.0 GPa, which are up to 4.5 times harder than the polycrystalline Au.³² An extrapolation³³ of the yield strength in the Hall–Petch relation (HPR) at submicron scales to the scaling laws for foamed materials has yielded the strength of 15 nm diameter ligaments to be 1.5 GPa, which is close to the theoretical strength of Au. Similarly, the strength of Al foams can be increased by 60%–75% upon thermal treatment and age hardening after foaming.³⁴ The Al foam is found to be twice as strong as pure Al, and the hardness decreases with increasing temperature.³⁵ However, the porous structure is thermally less stable. The local melting temperatures show a strong dependence on the void size.³⁶

Despite these exciting prospects, a consistent understanding of the mechanical strength and the thermal instability of voided structures at the nanoscale is highly desirable.³⁷ Here, we show with analytical solutions that the shortened and strengthened bonds between the undercoordinated atoms in the negatively curved surface skins dominate the observed nanocavity strengthening and thermal instability.

II. PRINCIPLE

A. Extended bond-order–length–strength correlation

Because the mechanical behavior of a surface is quite different from that of the bulk interior,³⁸⁻⁴⁰ the effective elastic constants of a nanofoam need to be considered in terms of a three-phase structure, i.e., the bulk matrix, the voids, and the interface skins between voids and matrix⁴¹ (see Fig. 1). The effects of pore size, bond nature, temperature, and, in

particular, the large portion of the undercoordinated atoms play significant roles in the mechanical properties of porous materials.

The bond-order–length–strength (BOLS) correlation mechanism^{42,43} indicates that if one bond breaks, the neighboring ones become shorter and stiffer. As such, a local strain and a potential well of trapping are generated at sites surrounding the broken bonds or at the surfaces of various curvatures. Naturally, the undercoordinated atoms surrounding atomic vacancies, point defects, nanocavities, and voids in nanofoams exactly perform the same to the undercoordinated atoms at the positively curved surfaces of nanostructures or at a flat surface despite the slight difference in the coordination environment. The extent of mechanical enhancement or thermal stability depression is determined by the portion of such undercoordinated atoms. Therefore, we can extend the BOLS correlation mechanism to the negatively curved surfaces of porous structures.

B. Analytical expressions

1. Surface-to-volume ratio

Considering a sphere of K radius with $(n+1/2)$ spherical cavities of L radius, as illustrated in Fig. 1, lined along the radius, the total number of voids is $4\pi(n+1/2)^2/3$. K and L are the dimensionless forms of size representing the number of atoms lined along the radius of the sphere and the hollow void, respectively. For a hollow sphere ($n=0$) with only one void in the center, this expression needs a slight revise. We can estimate the matrix volume V_0 occupied by atoms, the volume sum of the negatively curved skins of all the voids and the outermost surface skin of the sphere, V_i , the porosity p , and the mass density ρ_f by using the following relations:

$$V_0 = \frac{4\pi}{3} \left[K^3 - \frac{4\pi}{3} \left(n + \frac{1}{2} \right)^3 L^3 \right] \quad (\text{occupied-volume}),$$

$$V_i = 4\pi \left[K^2 C_{iK} + \frac{4\pi}{3} \left(n + \frac{1}{2} \right)^3 L^2 C_{iL} \right] \quad (\text{skin-volume}),$$

$$p = \frac{V_i}{V_0} = \frac{4\pi}{3} \left(n + \frac{1}{2} \right)^3 (L/K)^3 \\ = 1 - \rho_f \quad (\text{porosity-density}),$$

$$C_i = 2/\{1 + \exp[(12 - z_i)/(8z_i)]\} \quad (\text{bond-contraction}), \quad (1)$$

where C_{iL} and the C_{iK} represent the bond contraction coefficients for negatively curved surfaces of the L -sized voids and the positively curved surface of a K -sized sphere, respec-

tively. The subscript i denotes the atom in the i th atomic layer counted from the surface to the center of the solid.

For the curvature dependence of the effective atomic coordination (CN), an empirical relation could be derived from Refs. 44 and 45 for metals and silicon by assuming the effective bulk value of 12,

$$z_1 = 4(1 \pm 0.75/K), \quad z_2 = z_1 + 2, \quad \text{and} \quad z_{i \geq 3} = 12. \quad (2)$$

The $(-)$ sign is for the positively curved surfaces and the $(+)$ sign for the negatively curved surfaces. The effective bulk CN is different from the apparent CN such as in the diamond structure of Si. The diamond structure is actually an offset of two fcc lattice, so the effective bulk CN is 12 in-

stead of 4. For a flat surface, the apparent CN is 4 rather than 6. Considerable experimental evidence shows that the first atomic layer contracts by around 10%–15%, which corresponds to an effective CN of 4 (for further discussion, please refer to Ref. 42). Even at a liquid Sn surface, a 10% contraction of the spacing between the first and the second atomic surface layers was detected by using the x-ray reflectivity measurements.⁴⁶ The accuracy of Eq. (4) may lead to a slight deviation in estimation but not the nature of the phenomenon.

The ratio between the volume sum of the skins and the volume of the matrix can be expressed in a vector form, $r_i(n, L, K) = [\gamma_{iK}(C_{iK}), r_{iL}(C_{iL})]$,

$$r_i(n, L, K) = \frac{3C_{iK} + \frac{4\pi}{3}\left(n + \frac{1}{2}\right)^3 (L/K)^2 C_{iL}}{K \left[1 - \frac{4\pi}{3}\left(n + \frac{1}{2}\right)^3 (L/K)^3\right]} = \frac{3C_{iK}, 4\pi\left(n + \frac{1}{2}\right)^3 (L/K)^2 C_{iL}}{K \left[1 - \frac{4\pi}{3}\left(n + \frac{1}{2}\right)^3 (L/K)^3\right]} \quad (3)$$

$$= (\gamma_{iK}, \gamma_{iL}) = \frac{3}{K_j} \begin{cases} C_{iK} & \text{(solid-sphere: } L=0) \\ \frac{3C_{iK} + \frac{4\pi}{3}\left(n + \frac{1}{2}\right)^3 (L/K)^2 C_{iL}}{1 - \frac{4\pi}{3}\left(n + \frac{1}{2}\right)^3 (L/K)^3} & \text{(porous-sphere)} \\ \frac{C_{iK} + (L/K)^2 C_{iL}}{1 - (L/K)^3} & \text{(hollow-sphere)} \end{cases}$$

The parameters n , L , and K are constrained by the relation $2(L+1)(n+1/2) \leq K-1$ because a limited number of cavities can be lined along the radius K . The term $2(L+1)$ represents the diameter of the void including the one layer of surface skin and $K-1$ represents the radius of the sphere without the skin surface. This expression covers situations of a solid sphere and a sphere with uniformly distributed cavities of the same size. A similar form for the hollow sphere is also given with a minor correction for the general expression. This expression can be extended to a solid rod, a hollow tube, and a porous nanowire as well.

With the derived surface-to-volume ratio, $r_i(n, L, K)$, and the given expressions for the density of a certain quantity Q at the specific i th atomic layer site,⁴² $q_i(z_i, d_i, E_i)$, one can readily predict the size, cavity density, and temperature dependence of a detectable quantity Q of a system by using the given scaling relation

$$\frac{\Delta Q(K)}{Q(\infty)} = \sum_{i \leq 3} \gamma_i \frac{\Delta q_i(K)}{q(\infty)}. \quad (4)$$

The sum is over the outermost two atomic layers from the vacancy to the center of the matrix because the coordination deficiency is negligible for $i > 3$.

2. Thermal stability and elasticity

It is understood that the local melting point T_{mi} at a specific atomic site is proportional to the atomic cohesive energy, or the product of the atomic CN and the cohesive energy per bond, $T_{mi} \propto z_i E_i$, and that the local elastic modulus is proportional to the energy density, $Y_i \propto E_i / d_i^3$.⁴² With the given relations for T_{mi} and Y_i , we can estimate the relative changes in T_m and Y of a nanovoided specimen to those of the bulk by using the local bond average method represented with Eq. (4),

$$\frac{\Delta T_m(m, n, K, L)}{T_m(m, 0, \infty, 0)} = \sum_{i \leq 3} (r_{iK}, r_{iL}) \left(\frac{z_{iKb} C_{iK}^{-m} - 1}{z_{iLb} C_{iL}^{-m} - 1} \right),$$

$$\frac{\Delta Y(T, m, n, K, L)}{Y(0, m, 0, \infty, 0)} = \frac{1}{(1 + \alpha T)^3} \sum_{i \leq 3} (r_{iK}, r_{iL}) \left(\begin{array}{c} C_{iK}^{-(3+m)} \left(1 - \frac{\int_0^T \eta_1(t) dt}{z_{iKb} C_{iK}^{-m} E_b(0)} \right) - 1 \\ C_{iL}^{-(3+m)} \left(1 - \frac{\int_0^T \eta_1(t) dt}{z_{iLb} C_{iL}^{-m} E_b(0)} \right) - 1 \end{array} \right), \quad (5)$$

where m is the bond nature indicator and $E_b(0)$ is the cohesive energy per bond at 0 K. $z_{iLb} = z_{iL}/z_b$ and $z_{iKb} = z_{iK}/z_b$ with $z_b = 12$ as the effective bulk standard of atomic CN. $\eta_1(t)$ is the specific heat per bond, which was assumed to follow the Debye approximation. In reality, $\eta_1(t)$ deviates from the ideal Debye approximation by several percentages.⁴² The integration $\int_0^T \eta_1(t) dt$ is the internal energy of the specific bond, or the thermal energy for bond vibration. The calculation sums over the skin of the two atomic layers.

3. Inverse Hall–Petch relationship

Mechanical strengthening with grain refinement in the size range of 100 nm or larger has traditionally been rationalized with the so-called T -independent HPR that can be simplified in a dimensionless form normalized by the bulk strength, $\sigma(\infty)$, measured at the same temperature and under the same conditions:

$$\sigma(K_j)/\sigma(\infty) = 1 + AK^{-0.5}. \quad (6)$$

The slope A is an adjustable parameter for experimental data fitting, which represents both the intrinsic properties and the extrinsic artifacts such as defects, the pileup of dislocations, shapes of indentation tips, strain rates, load scales, and directions in the test.

As the crystal is refined from the micrometer regime into the nanometer regime, the classical HPR process invariably breaks down and the yield strength versus grain size relationship markedly departs from that seen at larger grain sizes—inverse HPR (IHPR) occurs. With further grain refinement,

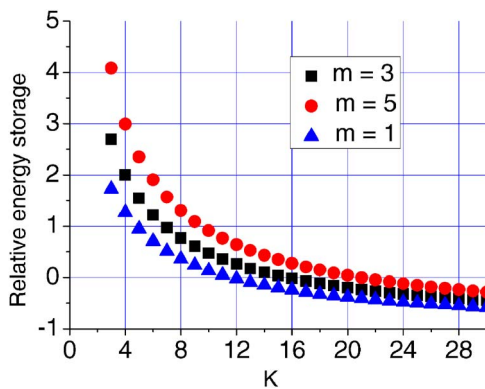


FIG. 2. (Color online) Prediction of the bond nature dependence of the critical pore size below which the total energy stored in the atomic shells of the hollow sphere is greater than the energy stored in an ideal bulk of the same size. m is the bond nature indicator, which is optimized as 2.56 for carbon (Ref. 12) and 4.88 for silicon (Ref. 42).

the yield stress peaks in many cases at a mean grain size on the order of 10 nm or so. A further decrease in grain size can cause softening of the solid instead, and then the HPR slope turns from positive to negative at a critical size, or the so-called strongest grain size.⁴⁷ The IHPR can be expressed as⁴⁸

$$\frac{\sigma(K, T)}{\sigma(\infty, T)} = \left\{ 1 + A' \exp \left[\frac{T_m(K)}{T} \right] K^{-1/2} \right\} \times \left\{ \left[\frac{d(\infty)}{d(K)} \right]^3 \left[\frac{T_m(K) - T}{T_m(\infty)} \right] \right\}, \quad (7)$$

where A' is a prefactor and $T_m(K)$ represents the melting point of the porous structure $T_m(m, n, K, L)$ and $T_m(\infty)$ is for the bulk. The reduced bond length is given as

$$d(K)/d = 1 + \sum_{i \leq 3} (r_{iK}, r_{iL}) \left(\frac{C_{iK} - 1}{C_{ii} - 1} \right).$$

The two parts in Eq. (7) represent that the IHPR originates from two competitions. One is the extrinsic competi-

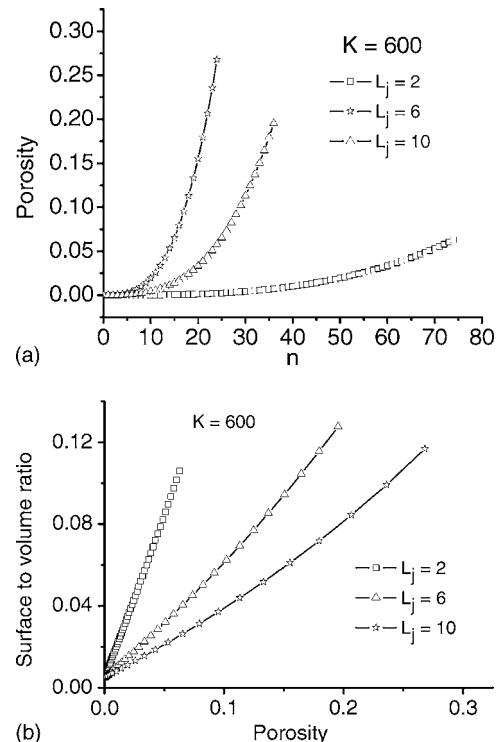


FIG. 3. Relationship between (a) the number of cavities and the porosity and (b) the relationship between the porosity and the surface-to-volume ratio for different pore sizes (L) in a $K=600$ sized sphere.

tion between activation ($\propto \exp[T_m(K)/T]$) and prohibition ($\propto A'K^{-1/2}$) of atomic dislocations and the other is the intrinsic competition between the temperature-dependent energy-density-gain ($\propto [T_m(K) - T]/d^3(K)$) in the surface skin and the residual cohesive energy [$\propto T_m(K)$] of the undercoordinated surface atoms. The activation energy is proportional to the atomic cohesion, which drops with solid size, whereas the prohibition of atomic dislocation arises from dislocation accumulation and strain gradient work hardening, which increases with the indentation depth. As the solid size is decreased, a transition from dominance of energy-density-gain to dominance of residual cohesive energy occurs at the IHPR

strongest size because of the increased portion of undercoordinated atoms. During the transition, contributions from both processes are competitive.

III. RESULTS AND DISCUSSION

A. Energy storage in hollow structure: Critical size

Assuming a hollow sphere of K exterior radius with a shell of $C_{1L} + C_{1K}$ thick, or three contracted atomic layers, we have the total energy stored in the shell skin at 0 K in comparison to that stored in an ideal solid sphere without surface effect as

$$\frac{\Delta E_{\text{shell}}}{E_{\text{sphere}}} = \frac{C_{1L}^{-(m+3)} \int_{K-(C_{1L}+C_{1K})}^{K-C_{1K}} 4\pi R^2 dR + C_{1K}^{-(m+3)} \int_{K-C_{1K}}^K 4\pi R^2 dR}{\int_0^L 4\pi R^2 dR} - 1 = C_{1L}^{-(m+3)} [(1 - C_{1K}/K)^3 - (1 - (C_{1L} + C_{1K})/K)^3] + C_{1K}^{-(m+3)} [1 - (1 - C_{1K}/K)^3] - 1. \quad (8)$$

Calculations were conducted based on the given $C_i(z_i)$ relation and the curvature dependent z_i values in Eqs. (1) and (2). From the results shown in Fig. 2, we can find the critical size below which the total energy stored in the shell of a hollow sphere is greater than that stored in a solid sphere of the same size. The estimation indicates that the critical size is bond nature dependent. The critical radius for a hollow sphere are estimated to be $K=12, 16,$ and 20 for $m=1$ (metal), 3 (carbon, 2.56), and 5 (Si, 4.88), respectively. Similarly, for hollow tubes, the corresponding critical K values are estimated at $7, 10,$ and 14 . For a single-walled hollow structure, the integration crosses only the diameter of the wall atom. It is emphasized that the elasticity of the shell is always higher than that of the bulk interior because elasticity is proportional to the energy density, $C_i^{-(m+3)}$. However, in plastic deformation, a hollow sphere could be tougher than a solid bulk structure because of the long range effect in the indentation deformation test. No dislocation accumulation occurred in the direction of the surface normal of the walls. On the other hand, the thermal stability of a hollow nanosphere is always lower than that of a solid sphere because of the high portion of the undercoordinated atoms.

B. Porosity dependence of elasticity and thermal stability

Figure 3 shows the surface-to-volume ratio as a function of porosity and the relative size of L/K . It can be seen that the smaller the cavities are, the larger the values of the surface-to-volume ratio are. Calculations of the Y and T_m were conducted by using a fixed value of sphere radius $K=600$ with different L and n values and a fixed $m=1$ for metals.

Figure 4 shows that T_m drops when the porosity is increased; at the same porosity, a specimen with a smaller pore size is thermally less stable. Young's modulus increases with the porosity and Young's modulus of a specimen with smaller pores increases faster. The predicted trends of thermal stability and strength agree well with the experimental

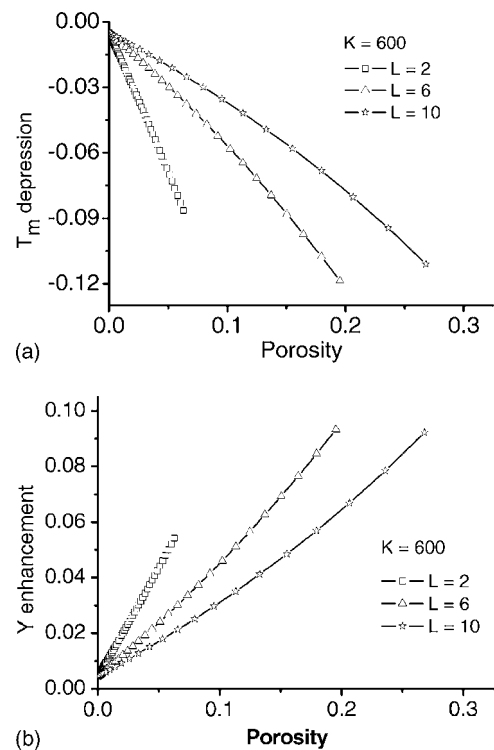


FIG. 4. Prediction of the porosity dependence of (a) T_m and (b) Y with different pore sizes in a $K=600$ porous specimen.

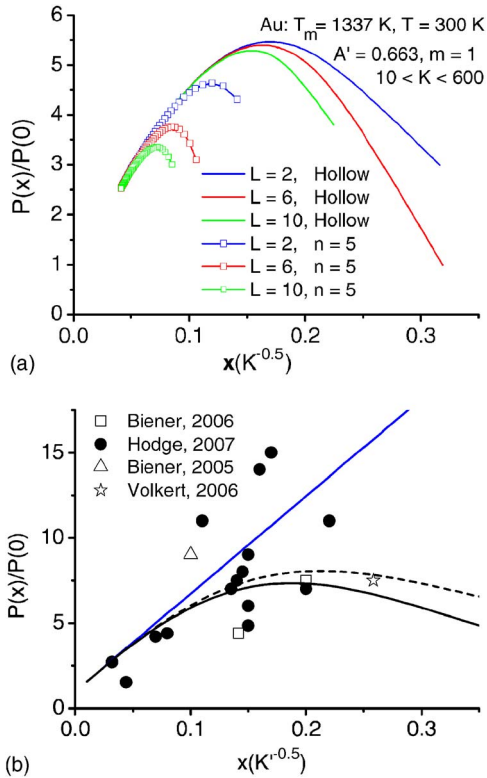


FIG. 5. (Color online) Prediction of (a) the IHPR for nanoporous Au spheres with radius varying from 10 to 600 with different numbers and sizes of the pores and (b) comparison of the predicted IHPR of Au with the measured data 1 (Ref. 28), data 2 (Ref. 27), data 3 (Ref. 31), and data 4 (Ref. 33). The ligament size $x(K^{-1/2})$ is derived from Au foams with the modified scaling relation of Gibson and Ashby (Ref. 2). The curve denoted HPR is the classical HPR and the curves denoted IHPR 2 and IHPR 1 are, respectively, the inverse HPR with and without the intrinsic competition of cohesive energy and energy density being involved, as discussed for the nanoparticles in the context.

observations of the size-dependent mechanical properties of nanoporous Au (Refs. 32 and 49) and the polymer hollow fibers.¹¹ It is important to note that there exists a limit of porosity because of the constraint as discussed above.

C. Plastic deformation

In dealing with plastic deformation by using IHPR, we may introduce an effective K' for the effective size and the following relation to find the effective volume by excluding the pore volume in the specimen:

$$\frac{4\pi}{3}K'^3 = \frac{4\pi}{3} \left[K^3 - (n+1/2)^3 \frac{4\pi}{3} L^3 \right], \quad x = K'^{-1/2}. \quad (9)$$

Figure 5(a) shows the predicted IHPR as a function of L for $10 < K < 600$ specimens. Compared to the situation of a single nanoparticle, the strongest size is significantly reduced for foams. Figure 5(b) compares the predicted room temperature IHPR (Ref. 12) to the measured strength of the ligaments in Au foams. HPR is the classical HPR showing linear dependence of flow strength with the inverse square root of particle size. IHPR 2 and IHPR 1 are the IHPR with and without involving the intrinsic competition of energy density and atomic cohesive energy, as discussed in Eq. (7). The scattered data for Au ligaments smaller than 5 nm deviate

from the predicted IHPR. One possibility is the surface chemical passivation effect because of the higher chemical reactivity of small particles. Chemical passivation alters the nature of the surface bond that will enhance the strength of the bonds. A combination of the present IHPR with the scaling laws for foamed materials may describe the observed trends at larger porosities.

According to the currently developed understanding, the magnitude of $T_m - T$, or the ratio T/T_m , plays a key role in determining the relative strength. The T_m of Al (933.5 K) is lower than that of Au (1337 K), which explains why the relative strength of Al foam to Al bulk is lower than that of Au.

D. Further evidence

The fact that the enhancement of the internal stress of a -C films can be done by changing the sizes of nanopores through the bombardment of noble gases (Ar, Kr, and Xe) (Refs. 17 and 18) and that of Ni films by He-gas bubble production²¹ could provide further evidence for the proposed mechanism for nanocavity hardening. The voided amorphous carbon films have a uniquely intrinsic stress (~ 12 GPa) that is almost one order in magnitude higher than those found in other amorphous materials, such as a -Si, a -Ge, or metals (< 1 GPa).⁵⁰ By using extended near-edge x-ray-absorption fine structure and x-ray photoelectron spectroscopy, Lacerda *et al.*¹⁷ investigated the effect of the trapping of noble gases in the a -C matrix on the internal stress of a -C films and the energy states of the trapped gases. They found that the internal stress could be raised from 1 to 11 GPa by controlling the sizes of the pores within which noble gases are trapped. Meanwhile, they found an ~ 1 eV lowering (smaller in magnitude) of the core-level binding energy of the entrapped gases associated with a 0.03–0.05 nm expansion of the atomic distance of the trapped noble gases. The measured core-level shift is of the same order as those measured for noble gases implanted in Ge,⁵¹ Al,⁵² and Cu, Ag, and Au,^{53,54} and Xe implanted in Pd hosts.⁵⁵ The interatomic separation of Ar (Xe) increases from 0.24 (0.29) to 0.29 (0.32) nm when the stress of the host a -C is increased from 1 to 11 GPa.⁵⁶

Comparatively, an external hydrostatic pressure around 11 GPa could suppress the interplanar distance of microcrystalline graphite by $\sim 15\%$,⁵⁷ gathering the core/valence electrons of carbon atoms closer together. The resistivity of a -C films decreases when the external hydrostatic pressure is increased.⁵⁸ These results are in agreement with the recent work of Umamoto *et al.*,⁵⁹ who proposed a dense, metallic, and rigid form of graphitic carbon with similar characteristics. The effect of hydrostatic pressure is very much the same as the pore-induced internal stress using noble gas sputtering and implanting.

The binding energy weakening and atomic distance expansion of the entrapped gases clearly indicate that the gas-entrapped pores expand in size and the interfacial C–C bonds contract because of the bond order loss of the interfacial C atoms, which contribute to the extraordinary mechanical strength of the entire a -C films. The pore-induced excessive stress is expected to play the same role as the external hy-

drostatic pressure that cause densification, metallization, and strengthening of the graphite by lattice compression.

The stiffness and strength enhancement of a nanotube and fiber mats by irradiation with energetic particles^{15,16} also provides further evidence for the BOLS mechanism. The bombardment by energetic particles could break the existing intrawall bonds and generate interwall bonds. The broken bonds cause the local strain and trapping and the new interwall bonding will enhance the layer interaction compared to the initially weak interwall bonding. Both the broken bonds and the newly generated bonds contribute to the strength of the irradiated specimen.

Recent analysis¹¹ suggests that the coupling of the surface tension between the exterior and interior surfaces of the hollow tube dominates the strength of polymer hollow fibers. It has also been suggested that⁶⁰ the presence of two unsaturated electronic bands near the Fermi level oppositely responding to shear stress enhances the hardness of the voided systems. The mechanisms of surface tension coupling¹¹ and density variation⁶⁰ are favored by the currently discussed BOLS correlation mechanism, indicating that a given density of states will shift to a lower energy because of the broken bond depressed potential well of trapping.

IV. CONCLUSION

It is concluded that the undercoordinated atoms in the negatively curved surfaces of atomic vacancies, point defects, nanocavities, and syntactic foams are responsible for the strain hardening and thermal stability depression of negatively curved systems, being the same by nature to those in positively curved systems, such as nanorods, nanograins, and flat surfaces. Numerically, negatively curved systems differ from zero- or the positively curved systems only by the fraction of the undercoordinated atoms and the coordination environment that determines the extent of BOLS induced property change. Therefore, all derivatives and conclusions for a flat surface and a positively curved surface apply to negatively curved ones without needing modification though quantitative information can be both experimentally and theoretically obtained. It is also concluded that the nanopores play dual roles in mechanical strength. The smaller pores act as pinning centers because of the strain and the trapping; the larger pores provide sites for initiating structure failure under indentation test.

Note added in proof. While proofing this article, we have become aware of the findings of coordination dependence of Au-Au bond contraction [61] that extends only to the outermost two atomic layers of the nanocrystals and the finding that the Au-Au bond contraction depends less on the type of substrate support [62]. Low-temperature scanning tunneling microscopy/spectroscopy measurements and density functional calculations [63] revealed that the occupied density-of-states for Co nanoislands on Cu(111) surface exhibit a sizable downward energy shift associated with bond contraction as the island size decreases, providing direct evidence for the strain-induced edge trapping. These findings fall excitingly within the currently discussed BOLS quantification and also

provide evidence for the accuracy and reliability of the BOLS correlation.

ACKNOWLEDGMENTS

This project is supported by MOE (Grant No. RG14/06), Singapore and by the NSFC (Grant Nos. 10772157 and 10525211).

- ¹J. Yan, X. Ma, W. Zhao, H. Tang, C. Zhu, and S. Cai, *ChemPhysChem* **6**, 2099 (2005).
- ²L. J. Gibson and M. F. Ashby, *Cellular Solids: Structure and Properties*, 2nd ed. (Cambridge University Press, Cambridge, 1997).
- ³H. H. Fu, D. J. Benson, and M. A. Meyers, *Acta Mater.* **49**, 2567 (2001).
- ⁴J. B. Wachtman, in *Mechanical and Thermal Properties of Ceramics*, edited by J. B. Wachtman (NBS, Washington, 1963), p. 139.
- ⁵J. K. MacKenzie, *Proc. Phys. Soc., London, Sect. B* **63**, 2 (1950).
- ⁶R. W. Rice, *J. Mater. Sci.* **40**, 983 (2005).
- ⁷C. Kittel, *Introduction to Solid State Physics*, 6th ed. (Wiley, New York, 1986).
- ⁸N. M. Pugno and R. S. Ruoff, *Philos. Mag.* **84**, 2829 (2004).
- ⁹Y. A. Chang, L. M. Pike, C. T. Liu, A. R. Bilbrey, and D. S. Stone, *Intermetallics* **1**, 107 (1993).
- ¹⁰I. Kaplan-Ashiri, S. R. Cohen, K. Gartsman, V. Ivanovskaya, T. Heine, G. Seifert, I. Wiesel, H. D. Wagner, and R. Tenne, *Proc. Natl. Acad. Sci. U.S.A.* **103**, 523 (2006).
- ¹¹X. F. Wu and Y. A. Dzenis, *J. Appl. Phys.* **102**, 044306 (2007).
- ¹²C. Q. Sun, H. L. Bai, B. K. Tay, S. Li, and E. Y. Jiang, *J. Phys. Chem. B* **107**, 7544 (2003).
- ¹³E. W. Wong, P. E. Sheehan, and C. M. Lieber, *Science* **277**, 1971 (1997).
- ¹⁴M. Sammalkorpi, A. Krashennnikov, A. Kuronen, K. Nordlund, and K. Kaski, *Phys. Rev. B* **70**, 245416 (2004).
- ¹⁵J. A. Astrom, A. V. Krashennnikov, and K. Nordlund, *Phys. Rev. Lett.* **93**, 215503 (2004).
- ¹⁶A. Kis, G. Csányi, J.-P. Salvetat, T.-N. Lee, E. Couteau, A. J. Kulik, W. Benoit, J. Brugger, and L. Forró, *Nat. Mater.* **3**, 153 (2004).
- ¹⁷R. G. Lacerda, M. C. Dos Santos, L. R. Tessler, P. Hammer, F. Alvarez, and F. C. Marques, *Phys. Rev. B* **68**, 054104 (2003).
- ¹⁸C. H. P. Poa, R. G. Lacerda, D. C. Cox, S. R. P. Silva, and F. C. Marques, *Appl. Phys. Lett.* **81**, 853 (2002).
- ¹⁹C. S. Shin, D. Gall, N. Hellgren, J. Patscheider, I. Petrov, and J. E. Greene, *J. Appl. Phys.* **93**, 6025 (2003).
- ²⁰V. K. Luk, M. J. Forrestal, and D. E. Amos, *J. Appl. Mech.* **58**, 1 (1991).
- ²¹J. A. Knapp, D. M. Follstaedt, and S. M. Myers, *J. Appl. Phys.* **103**, 013518 (2008).
- ²²C. S. Dai, D. L. Wang, F. Ding, X. G. Hu, and Z. H. Jiang, *Rare Metal Mater. Eng.* **33**, 1 (2004).
- ²³D. C. Dunand, *Adv. Eng. Mater.* **6**, 369 (2004).
- ²⁴C. Körner and R. F. Singer, *Adv. Eng. Mater.* **2**, 159 (2000).
- ²⁵K. M. Hurysk, *MRS Symposia Proceedings No. 521* (Materials Research Society, Pittsburgh, 1998), p. 191.
- ²⁶See <http://en.wikipedia.org/wiki/Porosity> for porosity in earth sciences and construction.
- ²⁷A. M. Hodge, J. Biener, J. R. Hayes, P. M. Bythrow, C. A. Volkert, and A. V. Hamza, *Acta Mater.* **55**, 1343 (2007).
- ²⁸J. Biener, A. M. Hodge, J. R. Hayes, C. A. Volkert, L. A. Zepeda-Ruiz, A. V. Hamza, and F. F. Abraham, *Nano Lett.* **6**, 2379 (2006).
- ²⁹B. Wu, A. Heidelberg, and J. J. Boland, *Nat. Mater.* **4**, 525 (2005).
- ³⁰M. D. Uchic, D. M. Dimiduk, J. N. Florando, and W. D. Nix, *Science* **305**, 986 (2004).
- ³¹J. Biener, A. M. Hodge, A. V. Hamza, L. M. Hsiung, and J. H. Satcher, *J. Appl. Phys.* **97**, 024301 (2005).
- ³²A. M. Hodge, J. Biener, L. L. Hsiung, Y. M. Wang, A. V. Hamza, and J. H. Satcher, *J. Mater. Res.* **20**, 554 (2005).
- ³³C. A. Volkert, E. T. Lilleodden, D. Kramer, and J. Weissmuller, *Appl. Phys. Lett.* **89**, 061920 (2006).
- ³⁴D. Lehmkus and J. Banhart, *Mater. Sci. Eng., A* **349**, 98 (2003).
- ³⁵O. Kraft, D. Saxa, M. Haag, and A. Wanner, *Z. Metallkd.* **92**, 1068 (2001).
- ³⁶X. M. Bai and M. Li, *Nano Lett.* **6**, 2284 (2006).
- ³⁷J. Biener, A. M. Hodge, and A. V. Hamza, *Appl. Phys. Lett.* **87**, 121908 (2005).
- ³⁸M. Zhao, W. T. Zheng, J. C. Li, Z. Wen, M. X. Gu, and C. Q. Sun, *Phys. Rev. B* **75**, 085427 (2007).

- ³⁹J. E. Sader, *J. Appl. Phys.* **91**, 9354 (2002).
- ⁴⁰M. X. Gu, C. Q. Sun, Z. Chen, T. C. Au Yeung, S. Li, C. M. Tan, and V. Nosik, *Phys. Rev. B* **75**, 125403 (2007).
- ⁴¹L. K. Pan, C. Q. Sun, and C. M. Li, *Appl. Surf. Sci.* **240**, 19 (2005).
- ⁴²C. Q. Sun, *Prog. Solid State Chem.* **35**, 1 (2007).
- ⁴³C. Q. Sun, *Phys. Rev. B* **69**, 045105 (2004).
- ⁴⁴S. Schuppler, S. L. Friedman, M. A. Marcus, D. L. Adler, Y.-H. Xie, F. M. Ross, Y. J. Chabal, T. D. Harris, L. E. Brus, W. L. Brown, E. E. Chaban, P. F. Szajowski, S. B. Christman, and P. H. Citrin, *Phys. Rev. B* **52**, 4910 (1995).
- ⁴⁵M. G. Mason, *Phys. Rev. B* **27**, 748 (1983).
- ⁴⁶O. G. Shpyrko, A. Y. Grigoriev, C. Steimer, P. S. Pershan, B. Lin, M. Meron, T. Graber, J. Gerbhardt, B. Ocko, and M. Deutsch, *Phys. Rev. B* **70**, 224206 (2004).
- ⁴⁷J. Schiotz, F. D. DiTolla, and K. W. Jacobsen, *Nature (London)* **391**, 561 (1998).
- ⁴⁸C. Q. Sun, S. Li, and C. M. Li, *J. Phys. Chem. B* **109**, 415 (2005).
- ⁴⁹A. Mathur and J. Erlebacher, *Appl. Phys. Lett.* **90**, 061910 (2007).
- ⁵⁰C. H. P. Poa, R. G. Lacerda, D. C. Cox, F. C. Marques, and S. R. P. Silva, *J. Vac. Sci. Technol. B* **21**, 1710 (2003).
- ⁵¹B. J. Wacławski, J. W. Gadzuk, and J. F. Herbst, *Phys. Rev. Lett.* **41**, 583 (1978).
- ⁵²C. Biswas, A. K. Shukla, S. Banik, S. R. Barman, and A. Chakrabarti, *Phys. Rev. Lett.* **92**, 115506 (2004).
- ⁵³P. H. Citrin and D. R. Hamann, *Phys. Rev. B* **10**, 4948 (1974).
- ⁵⁴R. E. Watson, J. F. Herbst, and J. W. Wilkins, *Phys. Rev. B* **14**, 18 (1976).
- ⁵⁵G. Kaindl, T. C. Chiang, D. E. Eastman, and F. J. Himpsel, *Phys. Rev. Lett.* **45**, 1808 (1980).
- ⁵⁶R. G. Lacerda, L. R. Tessler, M. C. dos Santos, P. Hammer, F. Alvarez, and F. C. Marques, *J. Non-Cryst. Solids* **299**, 805 (2002).
- ⁵⁷R. W. Lynch and H. G. Drickamer, *J. Chem. Phys.* **44**, 181 (1966).
- ⁵⁸S. Bhattacharyya and S. V. Subramanyam, *Appl. Phys. Lett.* **71**, 632 (1997).
- ⁵⁹K. Umemoto, S. Saito, S. Berber, and D. Tomanek, *Phys. Rev. B* **64**, 193409 (2001).
- ⁶⁰S. H. Jhi, J. Ihm, S. G. Louie, and M. L. Cohen, *Nature (London)* **399**, 132 (1999).
- ⁶¹W. J. Huang, R. Sun, J. Tao, L. D. Menard, R. G. Nuzzo, and J. M. Zuo, *Nat. Mater.* **7**, 308 (2008).
- ⁶²J. T. Miller, A. J. Kropf, Y. Zha, J. R. Regalbutto, L. Delannoy, C. Louis, E. Bus, and J. A. van Bokhoven, *J. Catal.* **240**, 222 (2006).
- ⁶³M. V. Rastei, B. Heinrich, L. Limot, P. A. Ignatiev, V. S. Stepanyuk, P. Bruno, and J. P. Bucher, *Phys. Rev. Lett.* **99**, 246102 (2007).